Journal of Coastal Research	18	4	760–775	West Palm Beach, Florida	Fall 2002

Sand Volume Change and Cross-shore Sand Transfer, Mangawhai Beach, New Zealand

D. Murray Hicks†, Malcolm O. Green‡, R. Keith Smith‡, Andrew Swales‡, Ron Ovenden‡ and Jeremy Walsh†

†National Institute of Water and Atmospheric Research Ltd.
PO Box 8602
Christchurch, New Zealand

‡National Institute of Water and Atmospheric Research Ltd.
PO Box 11-115
Hamilton, New Zealand

ABSTRACT

HICKS, D. M.; GREEN, M.O.; SMITH, R. K.; SWALES, A.; OVENDEN, R., and WALSH, J., 2002. Sand volume change and cross-shore sand transfer, Mangawhai Beach, New Zealand. *Journal of Coastal Research,* 18(4), 760–775. West Palm Beach (Florida), ISSN 0749-0208.

Sand volumes and cross-shore sand transport within a swath of beach and shoreface at Mangawhai, Northland, New Zealand were monitored during six weeks of swell and storm waves in order to capture any significant sand exchanges between the beach and inner shelf. The main data-collection involved repeat surveys of sand levels over 16 profiles, evenly spaced along 500 m of shore and extending from dune-toe to 10–11 m depth. The upper beach was surveyed with Emery poles while a sea-sled was used for the shoreface. The sea-sled was equipped with tilt-sensors and a wheel so that the surveyed bed profile could be adjusted for mast-tilt and bedform effects. The spatial distribution of cross-shore sand fluxes was derived by integrating the sand level changes between consecutive surveys. Reference rods in the shoreface were used to verify the sled data and to identify depth of bed disturbance. An instrumented tripod was used to measure near-bed wave-orbital and steady-current velocities and sand concentrations and to compute sand fluxes at several points on the shoreface.

Results showed that during a swell-dominated accretionary phase, onshore sand fluxes were associated with shoreward migrating bars in the swash zone and on the upper beachface but were negligible on the shoreface. With waves generated by an extra-tropical cyclone, offshore fluxes peaked over the outer bar as it was translated seaward but appeared to pinch-out at about 8 m depth, as predicted from wave climate statistics by HALLERMEIER's (1981) model. This average pattern was confused at individual profiles by longshore gradients in sand transport associated with rip-channels, rhythmic topography, and non-uniform beach drainage. When averaged over the whole study swath, the differences in sand volume between surveys were small (1–4 m^3m^{-1}) and consistent with measurement error, suggesting that the beach-shoreface was essentially a closed system, with no significant sand exchange with offshore during the monitoring time frame.

ADDITIONAL INDEX WORDS: *Sand volumes, sea-sled, closure depth.*

INTRODUCTION

Most beach sand on the northeast coast of New Zealand's North Island is generally regarded as having been derived from shoreward reworking of continental shelf sands during late-Quaternary transgressions, albeit with some local recycling of backshore deposits into the nearshore (SCHOFIELD, 1970; HILTON, 1995). Studies of inner shelf and nearshore morphology and sedimentology suggest that the inner shelf has now substantially "run out" of beach-grade sand and is no longer a significant source of beach sand (HILTON, 1995; HESP and HILTON, 1996). This tends to be confirmed by historical records of shoreline movement, which indicate that most of these beaches are quasi-stable, neither accreting nor eroding over decadal time scales (GIBB, 1978; NORTHLAND REGIONAL COUNCIL, 1988 and 1991).

To help clarify whether there remains some sand replenishment from the continental shelf in this area, during March–April 1996 we studied sand volume changes and fluxes within a swath of beach and shoreface at Mangawhai (Figure 1), aiming to record any net changes in sand storage and sand fluxes that related to exchanges with the inner shelf during a reasonably typical cycle of beach accretion and erosion. The study swath spanned 500 m alongshore and extended 600 m offshore, from the foredune toe to near the base of the shoreface at approximately 11 m depth below mean sea level. The broad approach was to survey repeat 'snapshots' of beach and shoreface topography with a network of profiles, from which sand volumes and net cross-shore sand transfers between surveys could be inferred, and to supplement these with time-series data on sand fluxes obtained by an instrument package moved between several points on the shoreface during the survey period. When integrated over time, the sand flux measured by the instruments at the instrument station could be compared with that inferred from the sea-bed surveys.

This approach requires that several assumptions/conditions be met. The first is that the sea-bed levels are surveyed with sufficient accuracy. Since they involve spatial integration, estimates of sand volumes and of time-averaged cross-shore sand fluxes based on surveyed changes in sand levels

01040 received and accepted as a resubmitted paper 26 April 2001.

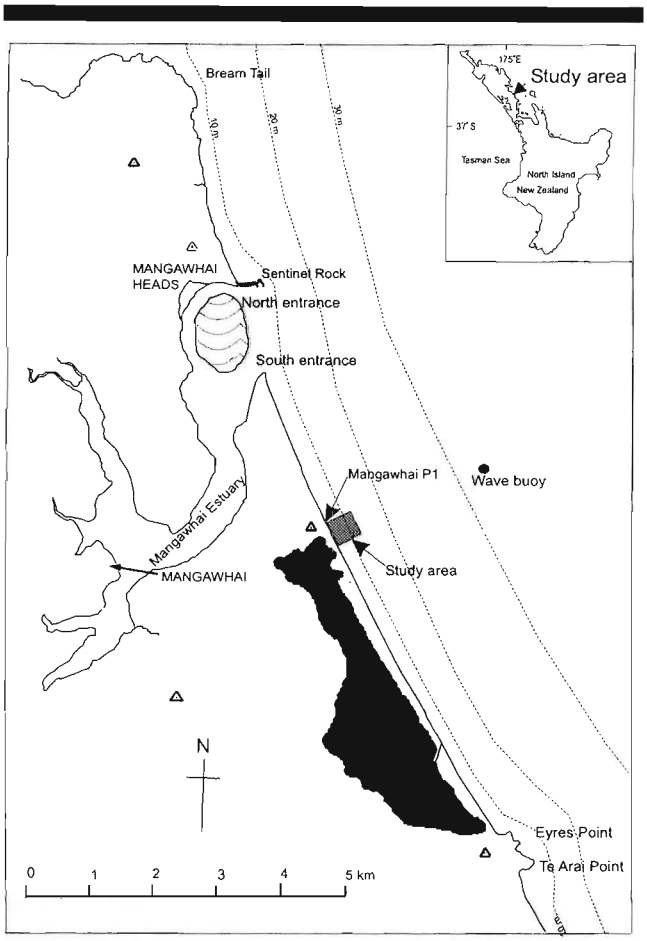

Figure 1. Map locating the study area on Mangawhai Beach, Outer Hauraki Gulf, North Island, New Zealand.

are highly sensitive to the accuracy of the surveying method, particularly any systematic errors. Seabed survey vehicles such as sleds provide much improved accuracy over traditional echo-sounding, but may still induce a bias in registration of the true sand-level due to the effects of sled tilt and bedforms (SMITH *et al.*, 1997). The second assumption concerns the alongshore uniformity of the beach topography and transport processes. This affects the span of shore and spacing of profiles required to obtain representative results. Also, 3-dimensional features (such as rip channels and associated depositional aprons) and longshore gradients in longshore transport rate can confuse cross-shore fluxes estimated from repeat surveys of sand levels along shore-normal profiles.

In this paper, we (i) present the results of the 1996 Mangawhai Beach study and explore the evidence for any local sand exchanges between the beach-shoreface and further offshore, (ii) evaluate the assumptions concerning survey accuracy, representativeness of profiles, and the effects of alongshore variability in topography on sand flux estimates, (iii) explore the implications of the findings for monitoring beach sand volumes and sand transfers generally, and (iv) compare the depth limits of profile change and cross-shore transport

Table 1. *Wave statistics at Mangawhai for total 32-month record from ENDECO buoy and for period of sled surveys in March-April 1996. Statistics are based on spectral analysis. The period is the spectral average period. The buoy was stationed at 35 m water depth. Included are the seaward and landward depth limits of Hallermeier's (1981) 'shoal' zone, as determined from equations (10) and (11).*

	16 March 1995–7 November 1997	9 March–16 April 1996
Mean significant wave height, H_s (m)	0.75	0.64
Standard deviation of H_s, σ (m)	0.59	0.52
Median H_s, H_{sm} (m)	0.57	0.53
0.137 percentile H_s, $H_{s0.137}$ (m)	4.0	3.7
Maximum H_s (m)	5.6	3.7
Absolute maximum wave height (m)	8.1	6.0
Mean period (s)	6.3	7.2
Median direction of maximum energy (degrees E of N)	064	066
Depth of seaward boundary, d_i (m from MSL)	10.8	10.7
Depth of landward boundary, d_l (m from MSL)	8.9	8.0

with these predicted by HALLERMEIER's (1981) equations. Related papers have reported on geostatistical features of the Mangawhai Beach topography (SWALES, submitted) and processes observed at the instrumented tripod, including initial motion (GREEN, 1999), the influence of bedforms on sand suspension (GREEN and BLACK, 1999), and the process model encapsulated by the fall-speed parameter (HICKS and GREEN, 1997).

STUDY AREA

Mangawhai Beach lies in the Mangawhai-Pakiri embayment on the east coast of the Northland Peninsula of New Zealand's North Island (Figure 1). It extends some 10 km south from Mangawhai Estuary. At the time of the study, the estuary had two entrances but the southern entrance was partially closed. The study site is some 3 km south of this southern entrance. The shore-normal at the study site is oriented 65° east of north.

The site is exposed to the north-east and south-east but protected from waves from the north, east and south by offshore islands and the Northland Peninsula. The dominant wind direction is from the north-west to south-west but this can change depending on the phase of the El Nino Southern Oscillation (ENSO). During the first four months of 1996 the Southern Oscillation Index had an average value of 5.75, which signifies a weak La Nina phase of the ENSO. The La Nina phase tends to allow cyclones of tropical origin to pass close to New Zealand, bringing strong north-easterly winds and often heavy rain to the east coast. As a result, the wave climate (as measured at 35 m water depth, Table 1) is characterised by infrequent storm waves and low northeast swell, typically less than 0.6 m in height. The highest waves are associated with sub-tropical cyclones, with heights over 8 m and periods up to 20 s. Tides are semi-diurnal, with a neap (spring) range of 1.5 (3.0) m. Tidal currents in the area are weak, except around headlands (HUME *et al.*, 2000). Most current activity is driven by winds and density stratification, resulting in dominantly longshore flows with speeds typically

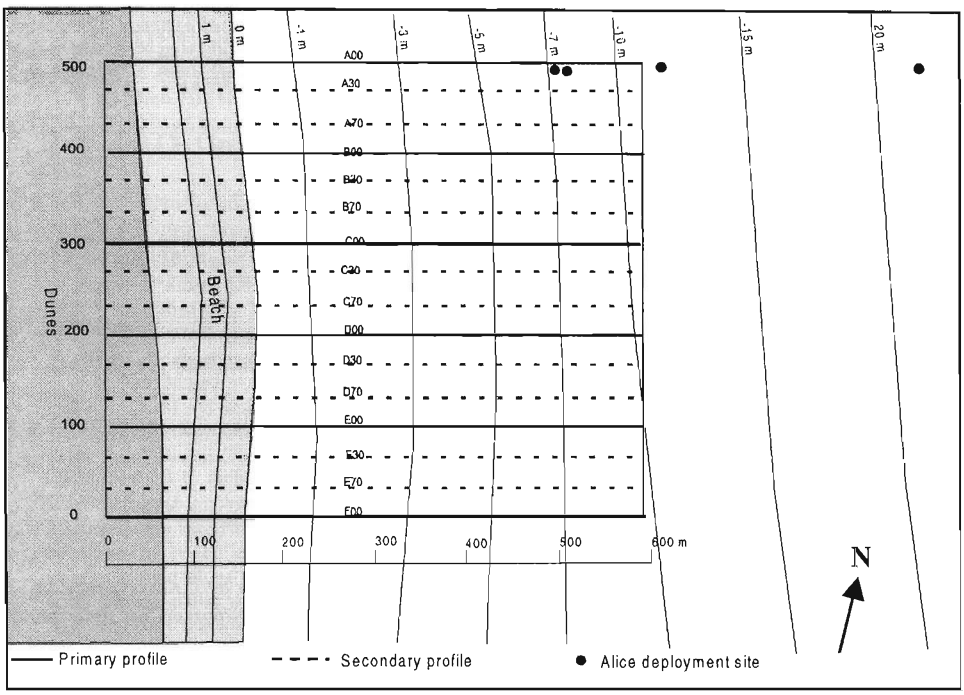

Figure 2. Layout of profiles across study swath on Mangawhai Beach, including stations where instrument tripod *Alice* was deployed.

less than 15 cm.s^{-1} and persisting over weather-band time scales (BLACK *et al.*, 2000). At depths greater than about 15 m, the coastal water column tends to stratify in the summer season, re-mixing during large storms.

Mangawhai Beach typically presents a trough/bar morphology which is either simple and straight or mildly rhythmic with weak rip cells developed. At approximately 22 m depth and 1 km offshore, the concave shoreface merges with the slightly convex inner continental shelf, which slopes seaward at 10 m.km^{-1}. The shoreface is composed of moderately well sorted fine-medium sand (median grainsize at 7 m depth on the shoreface is 0.2 mm). The inner shelf has less well sorted medium to coarse sand (MCCABE, 1985). The sands are predominantly quartzo-feldspathic with some rock and shell fragments. HILTON (1995) suggested that the shoreface sands in the Mangawhai-Pakiri littoral cell are derived from shoreward transport of the finer fractions of the inner shelf sediment since the end of the last transgression, and possibly also from storm erosion of older backshore sediment. HESP and HILTON (1996) concluded, mainly on the basis of morphological and sedimentological evidence, that the offshore sand source is now insignificant, although numerical modelling by HUME *et al.* (1999) indicated a "best estimate" shoreward sand flux of 12,000 m^{3}y^{-1} onto the Mangawhai-Pakiri shoreface. Nearshore sand has been mined from the Mangawhai-Pakiri embayment at rates of about 100,000 m^{3}y^{-1} in recent years. Based on two years of wave buoy records collected for the present study, HUME *et al.* (1999) estimated a net surf-zone longshore drift rate at Mangawhai of 47,000 m^{3}y^{-1} to the north and a gross drift of 267,000 m^{3}y^{-1}. The northward deflection of Mangawhai Inlet (Figure 1) suggests that net northward drift has prevailed over a longer time frame.

The beach is backed by sand dunes (ENRIGHT and ANDERSON, 1988). These are bare along the northern half of the study shore, but along the southern half the foredunes are vegetated in various dune species and the backshore lies in Mangawhai Forest, a plantation of *Pinus radiata*.

FIELD METHODS

Beach and Nearshore Topography Surveys

Sixteen equally spaced, shore-normal profiles were set up within the study swath (Figure 2). The longshore span and profile spacing were based on analysis of the semi-variance of elevation data from a preliminary survey which covered a full kilometre of the coast (SWALES, submitted). This showed rhythmic forms of about 500 m wavelength across the beach-shoreface, with finer topographic variation (< 100 m scale) on the beach above Mean Sea Level (MSL). We thus chose 100 m spacing for a primary set of profiles (labelled A00, B00 . . . F00), with secondary profiles (labelled A30, A70, B30, B70, etc) spaced at 30 m either side of the primary ones.

The sub-aerial beach, from dune toe to MSL, was surveyed daily between 7 March and 5 April and again on 15 and 17 April. The survey method was a variant of that of EMERY (1961), with a tape used to measure the distance between observation points. The lower segment of the profile, from the beach to 10–11 m depth, was surveyed using a sea-sled on four occasions (nominally 10 March, 20 March, 27 March, and

16 April, although each survey required several days to complete). On several of these occasions, deteriorating weather conditions prevented all 16 profiles being surveyed; in these circumstances, priority was given to the primary profiles.

The sea-sled design and operation are detailed in SMITH *et al.* (1997). Briefly, the sled has a 13 m mast topped with an EDM survey prism and is also equipped with a video camera, a biaxial inclinometer, and a digitising wheel. The inclinometer record allows the true offset and elevation of the base of the mast to be computed. The wheel records bedforms and permits the true bed profile to be referenced to the base of the sled (where bedforms are present, the track taken by the sled runners may not follow the true bed level, *i.e.,* they may be perched on top of firm ripples or they may cut through soft ripples). Output from the wheel and inclinometer was recorded on a data-logger every 0.5 s. The sled is towed offshore by a boat and is retrieved along the survey line by a diesel-powered hydraulic winch. During retrieval, a shore-based EDM (GEODIMETER 464) measures the position of the prism on the mast every 0.4 s. Repeat surveys a few hours apart indicated that the sled was able to fix seabed elevation to ± 10 mm (SMITH *et al.,* 1997). Retrieval speeds were typically 0.15–0.25 $m.s^{-1}$.

As a check on the sled surveys and to measure the depth of bed disturbance, arrays of 1.6 m long, 10 mm diameter aluminium "depth of disturbance" (DOD) rods were installed by diver along profiles A00 and F00 at water depths of approximately 2, 4, 6, 7, 8, 9, 10, and 15 m. Each array comprised five rods arranged at 1 m spacings in a 2 m by 2 m cross pattern. When the rods were installed, on 9–13 March, washers were placed at the sand level, the sand level was measured by pressing a white board on edge into the sand, and the sea floor was photographed. Sand levels against the rods were resurveyed on 23–25 March and on 16–19 April, with the washer depths measured during the latter survey. On each occasion, notes were made of bedforms, including the position of each rod with respect to adjacent bedforms, and sand samples were collected for grainsize analysis.

Instrumentation

Boundary-layer flows and sediment suspension were monitored with the instrumented tripod *Alice* (GREEN, 1996; GREEN, 1999) at several stations along the line of profile A00. *Alice* was equipped with vertical arrays of four Marsh-McBirney electromagnetic current meters and four D & A optical backscattering sensors, a pressure sensor, a video camera, sediment traps, and an acoustic backscatter sensor (ABS). The ABS measured suspended-sediment concentration profiles at 5 Hz for 10 min every hour. The other sensors burst-sampled every hour. *Alice* was deployed by helicopter, with diver assistance. The first deployment was at 12 m depth, from 19 February until 5 March. Subsequent deployments were at 7.0 m depth (11–14 March), 22 m depth (15–19 March), then back to 7.5 m depth (19–30 March). While at this last station on 30 March, *Alice* was tipped and rolled onto the beach by 6 m high waves generated by an extra-tropical cyclone. Fortunately, the storm data until this point were recovered.

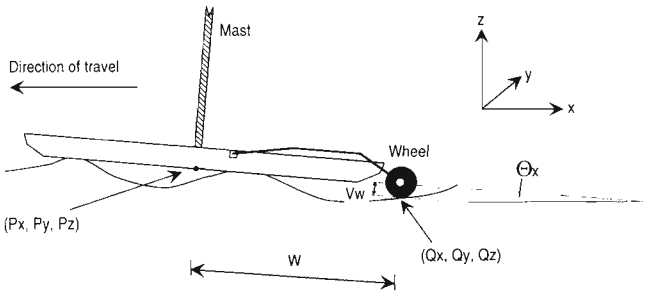

Figure 3. Sea-sled with digitising wheel traversing bedforms. Symbols as defined in text.

Waves were monitored every 2 hours through the study by an ENDECO directional buoy stationed at 35 m depth along the line of profile F00 (Figure 1). The full record of this wave buoy extends from March 1995 until November 1997. A wind recorder located on a backshore dune monitored wind speed and direction through the study period.

DATA REDUCTION

Profile Surveys

The sea-sled data underwent several stages of semi-automated reduction. The first stage involved using the sled's inclinometer record to derive the location of the base of the sled directly beneath the mast ($P_{x,y,z}$) from the position of the mast-top prism (as recorded by the EDM instrument). This procedure is detailed in SMITH *et al.* (1997). The second stage involved finding the position of the bed beneath the digitising wheel ($Q_{x,y,z}$), again using the inclinometer records. To a reasonable approximation, this was found as:

$$Q_x = P_x + W \cos \theta_x + V_w \sin \theta_x \qquad Q_y = P_y + U$$

$$Q_z = P_z - W \sin \theta_x + V_w \cos \theta_x \qquad (1)$$

where W is the inclined offset of the wheel from the centreline of the mast, U is the lateral offset of the wheel from the mast, V_w is the wheel offset measured normally to the plane of the sled base, and θ_x is the angle of sled tilt in the shore-normal direction (Figure 3).

The third stage involved de-spiking and smoothing the bed-level data. Spikes were identified and removed from the record when the elevation change from a smoothed (*i.e.,* by local averaging) profile exceeded a threshold value (typically, a 0.05 m threshold was found to give satisfactory results). The horizontal offsets were smoothed, using a running mean, to remove the "noise" generated by vibration and whiplash of the sled mast. This processed bed profile record and the synchronised record of bedform elevations (from the digitising wheel) were then interpolated at 37 mm intervals in horizontal position and added, thus giving the 'true' level of the bed at the position of the wheel. Finally, this combined signal was spilt into a smooth bed profile (trend) and a de-trended bedform signal using a 200 point running-mean.

It was found that bedforms induced a varying bias of the local mean elevation at the base of the sled runners from the

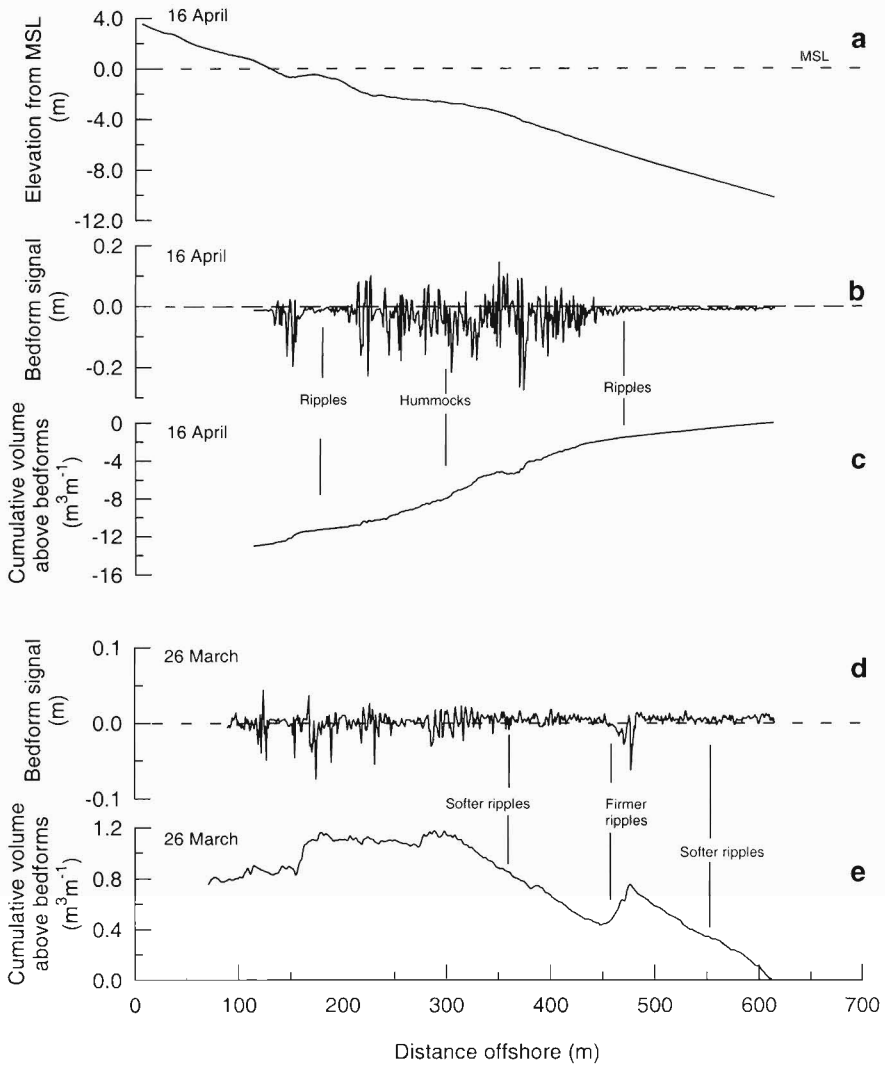

Figure 4. Sea-sled records from profile A00. (**a**) is the profile on 16 April, as determined from the surveyed level to the base of the sea-sled. (**b**) shows the bedform signal recorded by the digitising wheel on 16 April. (**c**) is the integral of the 16 April bedform signal, obtained by integrating curve b shoreward from a starting point at 610 m offshore, and so accumulates the sand volume difference (per m length of shore) between the smoothed sled-base profile and the true profile that includes the bedforms. (**d**) shows the bedform signal recorded by the digitising wheel on 26 March. (**e**) is the integral of the 26 March bedform signal.

true local mean bed elevation (Figure 4). Where the bed was rippled and the ripples were firm, the sled tended to be perched on the ripple crests. This induced a sled-base elevation averaging 5–10 mm higher than the true mean bed level (Figure 4b; see also SMITH *et al.*, 1997). When the ripples were formed of softer sand, the sled cut through them and this bias was reversed (Figure 4d). With hummocky / crescentic-dune topography (with bedform heights in the range 0.1–0.4 m and which was typically encountered on the seaward flanks of longshore bars in belts that widened as wave height increased), the sled's behaviour varied from ploughing-through to over-riding these bedforms. As a result, the bias in mean bed level was highly variable but tended to average out at several centimetres. When integrated over the 600+ m length of the Mangawhai profiles, this bias due to bedforms, if uncorrected, would have induced errors in total sand volume under the profiles of up to 13 m^3m^{-1} (Figures 4c and 4e) and would have added an accumulating bias to estimates of cross-shore sand fluxes (see below).

The reduced sled profiles were merged with the matching daily beach surveys to complete the profiles up to their benchmarks. Because the beach and sled surveys were not always completed at the same time of day, and beach levels changed locally by up to 0.1 m in the intervening period, the merging involved taking a weighted average of the overlapping ends of the beach and sled surveys.

The complete beach profiles were then used for two purposes: (i) to produce digital elevation models (DEMs) of the swath for morphologic and sand-volume analysis and (ii) to compute cross-shore sand fluxes. DEMs were created for each

survey using the kriging method to generate grids with 5 m node spacings in both the longshore and cross-shore directions. The DEMs from sequential surveys were differenced to highlight erosion and deposition. Also, a planar trend surface, sloping seaward at 1.27°, was subtracted from the original DEMs in order to highlight the superimposed bar, trough, and rip channel topography.

Following LARSON and KRAUS (1989), the distribution of net, time-averaged, cross-shore flux of sand over the beach and shoreface between consecutive surveys, $Q_{(x)}$, was found by integrating the surveyed elevation differences up the profile from its seaward end. Thus

$$Q_{(x)} = \int_{x_0}^{x} [z_2(x) - z_1(x)]\, dx \quad (2)$$

where z_1 and z_2 are the profile elevations at surveys 1 and 2 and x is the distance shoreward of the offshore point of zero change, x_0. By beginning the integration at the seaward limit of the surveyed part of the profile, it was assumed that there were no significant net cross-shore fluxes across this boundary. This assumption is reasonably justified if (i) the net cross-shore fluxes so calculated decay towards zero at this limit and (ii) the net flux at the landward end of the profile is small, and can be checked (within the uncertainty level of the surveys) by checking that mass is conserved across the profile.

Alice Data

The *Alice* data were processed to obtain estimates of burst-averaged wave parameters, suspended sand concentration, mean current speed and direction, and several higher-order moments of the instantaneous velocities. These results were then used to estimate burst-averaged net cross-shore flux of sand at the *Alice* site.

The suspended load, which was considered to be transported at elevations higher than 1 cm above the bed, was assumed to be entrained by the waves but transported by the mean current. Any net suspended load component induced by asymmetry in the instantaneous oscillatory currents (in the absence of any mean current) was ignored. This was justified on the basis that, at least for suspended load, the significance of this effect is far from clear amongst the complications added by phase-lag gradients in the boundary layer and bedform effects on sand suspension processes (*e.g.,* BLACK *et al.,* 1997). Likewise, any slope effects on the suspended load (such as appear in the total load transport models of INMAN and BAGNOLD, 1963, and BAILARD, 1981) were ignored due to the low seabed gradients (0.022) at the *Alice* sites. Accordingly, the vertically-integrated, burst-averaged fluxes of suspended sand transported by the mean current, Q_s ($kg.m^{-1}.s^{-1}$), were calculated from

$$Q_s = \int_{1\,cm}^{300\,cm} U_{(z)} C_{(z)}\, dz \quad (3)$$

where z is elevation above the bed and 1 and 300 are the integration limits in centimetres.

The burst-averaged concentration profile, $C_{(z)}$, was represented by

$$C_{(z)} = C_0 \exp(-z/l_s) \quad (4)$$

C_0 is a bed reference concentration which GREEN and BLACK (1999) found was related to the dimensionless skin friction, Θ', corrected for acceleration effects over ripples. The mixing length l_s was found to equal 60 cm with hummocky bedforms and 10 cm with a rippled bed (the two mutually exclusive bedform states observed at the *Alice* sites). The transition from ripples to hummocky topography was observed to occur when Θ' exceeded 0.14 (GREEN and BLACK, 1999).

The velocity profile, $U_{(z)}$, was estimated by

$$U_{(z)} = \frac{U^*}{\kappa} \ln\left(\frac{z}{z_0}\right) \quad (5)$$

where U^* is the burst-averaged friction velocity, κ is the von Karman constant, and z_0 is the hydraulic roughness. After SOULSBY (1983), z_0 was taken as

$$z_0 = 2H\,(H/L)^{1.4} \quad (6)$$

H and L, the height and wavelength of the bedforms, were estimated from the *Alice* video record, giving $z_0 = 0.08$ cm when the bed was rippled and $z_0 = 0.8$ cm when it was hummocky. Thus for each burst, once the type of bedform was established from Θ', the mean velocity profile could be determined from equations (5) and (6) and using the velocity from one of the current meters. The direction of the mean current was taken as the burst-averaged direction averaged from all four current meters. The cross-shore component of the mean current was obtained by multiplying by the unit vector in the cross-shore direction, i (positive offshore).

Bedload, Q_b ($kg.m^{-1}.s^{-1}$), assumed to be transported by the instantaneous orbital currents augmented by any mean current, was estimated from the bedload term of BAILARD's (1981) model as

$$Q_b = \frac{\rho_s}{(S_s - 1)g} C_f \epsilon_b \langle U_t^3 \rangle / (\tan\phi - \tan\beta) \quad (7)$$

where $\langle U_t^3 \rangle$ is the burst-averaged cube of the velocity, ρ_s is the sand density (2.65 $g.cm^{-3}$), S_s is ρ_s/ρ, ρ is water density, g is the gravitational acceleration, C_f is the friction coefficient for rough oscillatory flow (assumed equal to 0.003 after STERNBERG, 1972), ϵ_b is the bedload transport efficiency (set equal to 0.21 after BAILARD, 1981), ϕ is the friction angle ($\tan\phi$ taken as 0.63, after GUZA and THORNTON, 1985), and $\tan\beta$ is the cross-shore slope. As with the suspended load, the slope term in equation (7) was ignored since $\tan\phi >> \tan\beta$ at the *Alice* deployment sites. The component of the bedload due only to the orbital asymmetry (*i.e.* without any added mean current), $\langle U_w^3 \rangle$, was found by substituting $\langle (U_t - \langle U \rangle)^3 \rangle$ for $\langle U_t^3 \rangle$ in equation (7), where $\langle U \rangle$ is the burst mean velocity. The cross-shore component of the bedload was taken as $i \cdot Q_b$. Sand transport was assumed to be zero at sub threshold-of-motion conditions, as defined by the formula of KOMAR and MILLER (1973) using the definitions of significant wave height and mean spectral period recommended by GREEN (1999) and a representative grainsize of 0.2 mm for the shoreface sand.

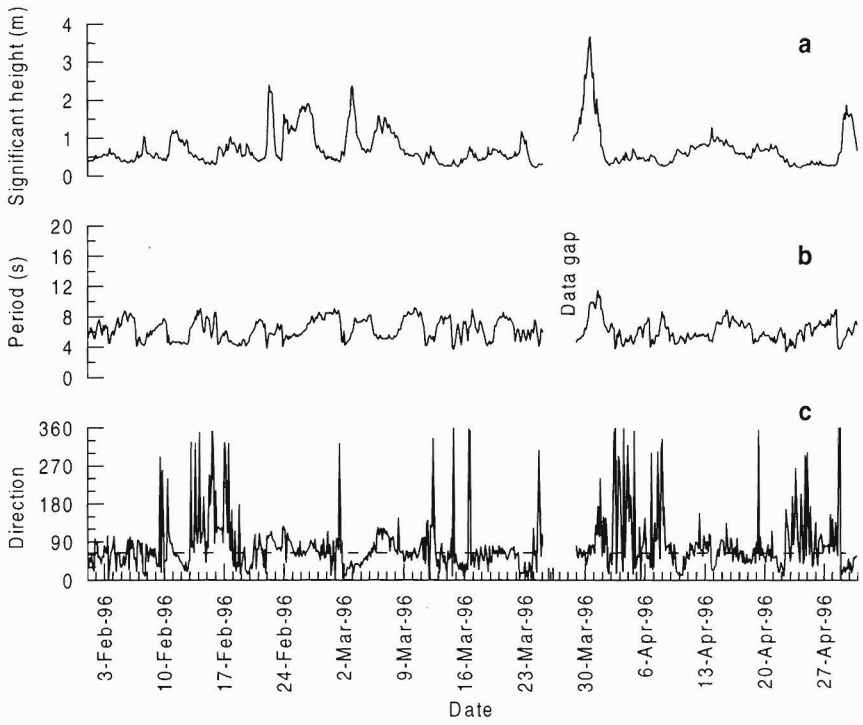

Figure 5. Wave conditions February through April 1996 at the Mangawhai wave buoy, located in 35 m water depth. (**a**) is significant height, (**b**) is spectral mean period, (**c**) is arrival direction of maximum energy.

RESULTS

Wave, Wind, and Current Conditions During the Study

Sea conditions measured by the ENDECO buoy at 35 m depth in the weeks before and during the study are shown in Figure 5. For much of the time, winds were light and the waves were low with significant height (H_s) of 0.5–1.0 m and mean spectral period (T_s) typically around 8–9 s. The swell direction varied but tended to be from the northeasterly quarter (on the northern side of shore normal) through most of March. Small-moderate events associated with passing depressions, occurring on February 22 and 24–27, and March 2–3, 6–7 and 22, were distinguished by shorter periods and higher waves. These waves generally arrived from either the southeast or northeast, at a significant angle to the shore-normal, and wave/wind-driven longshore currents were observed in the surfzone. From 30 March to 1 April, extra-tropical Cyclone Betty brought waves that increased progressively in height and period, with H_s peaking at almost 4 m and T_s peaking around 11 s. The maximum wave height recorded (H_{max}) was 6.0 m. The waves and winds were essentially onshore as this storm built but quartered to the southeast as it waned. The most substantial wave event prior to the study period occurred on 24 January 1996. This, too, was due to an extra-tropical cyclone and at its peak had H_s = 4.3 m, H_{max} = 5.6 m, and T_s = 13 s. The *Alice* records showed that mean currents on the shoreface-inner shelf (1 m above the bed) were predominantly directed alongshore (to the north or south, depending on the wind direction) at speeds typically a few $cm.s^{-1}$, but rose to at least 0.3 $m.s^{-1}$ during the cyclone (HICKS and GREEN, 1997).

Morphologic Change

The above sea conditions induced a cycle of morphologic change on the study swath (Figures 6 and 7). When the detailed surveys commenced in early March, the beach was recovering from an eroded, flattened state induced both from the late January cyclone and the short periods of rough weather in the preceding two weeks. At that stage, it had a longshore-bar-and-trough form. Through the rest of March, apart from some brief erosive setbacks, the beach generally accreted and bars in the swash zone and on the upper beachface migrated shoreward. As this phase proceeded, a mildly rhythmic beach topography developed as rip channels cut through the swash bar. The storm waves at the end of March flattened the beach and shifted the outer bar seaward, casting aprons of sand down the shoreface. In terms of the Wright-Short morphodynamic model (WRIGHT and SHORT, 1984), the beach began in the intermediate "longshore bar-trough" state, but by 20 March this had evolved more into the "rhythmic bar and beach" state. Both states are characteristic of accretion on a previously dissipative profile. With the March 30–31 cyclone, the beach flattened into a dissipative state but subsequently returned to the longshore bar-trough state.

A more detailed description of the morphologic change fol-

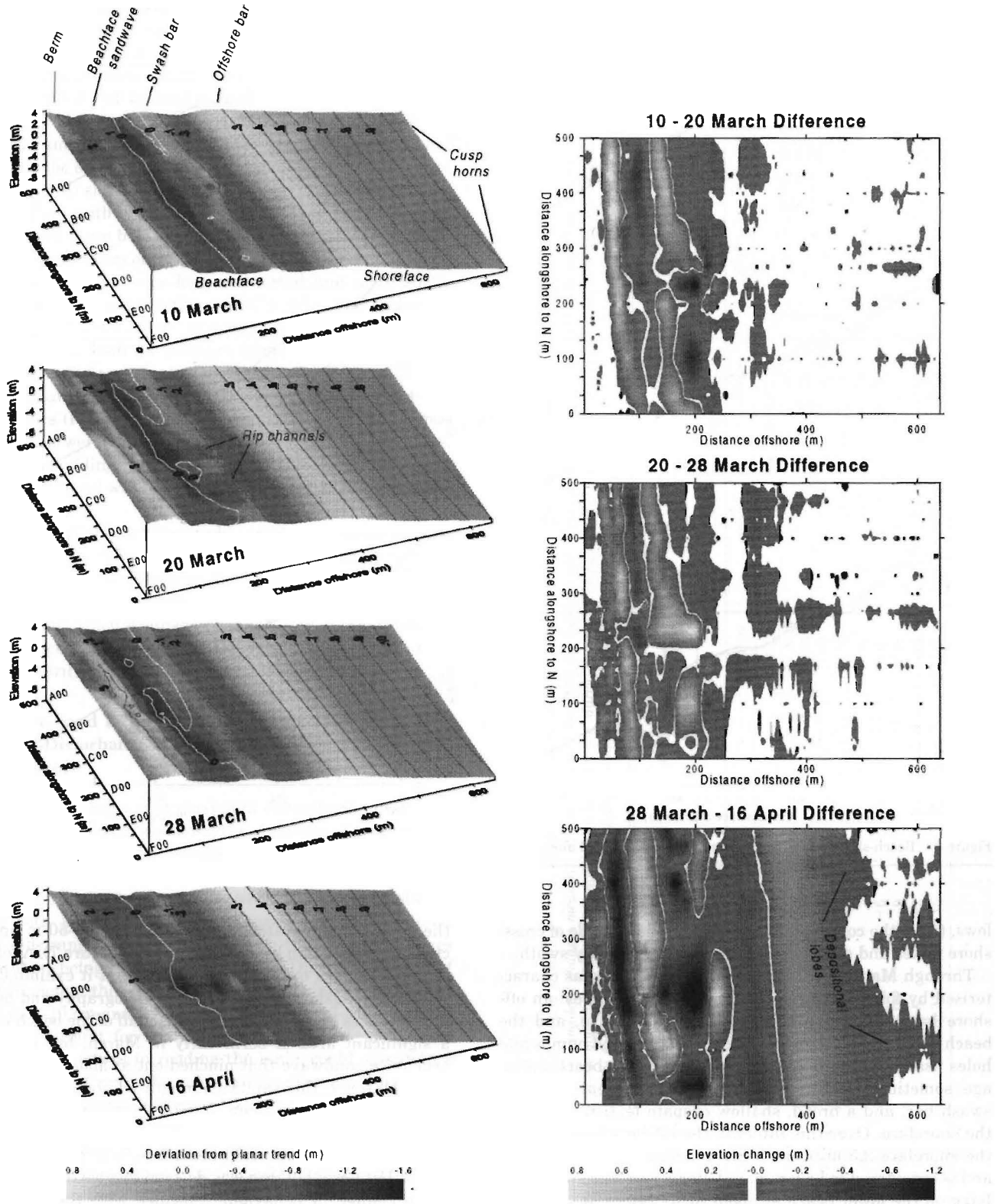

Figure 6. Beach and shoreface morphology and changes in elevation between surveys. On the 3-d plots: the shading scales the deviation of the actual topography from a seaward-sloping plane (common for all surveys), thus it highlights bar features rather than the absolute elevation; the contours (metres from MSL, marked by the white contour) indicate the true elevation; the primary profiles are labelled A00, B00, etc. On the elevation difference maps: areas in white indicate elevation changes less than ± 2 cm; cross-shore lineations are artifacts of gridding.

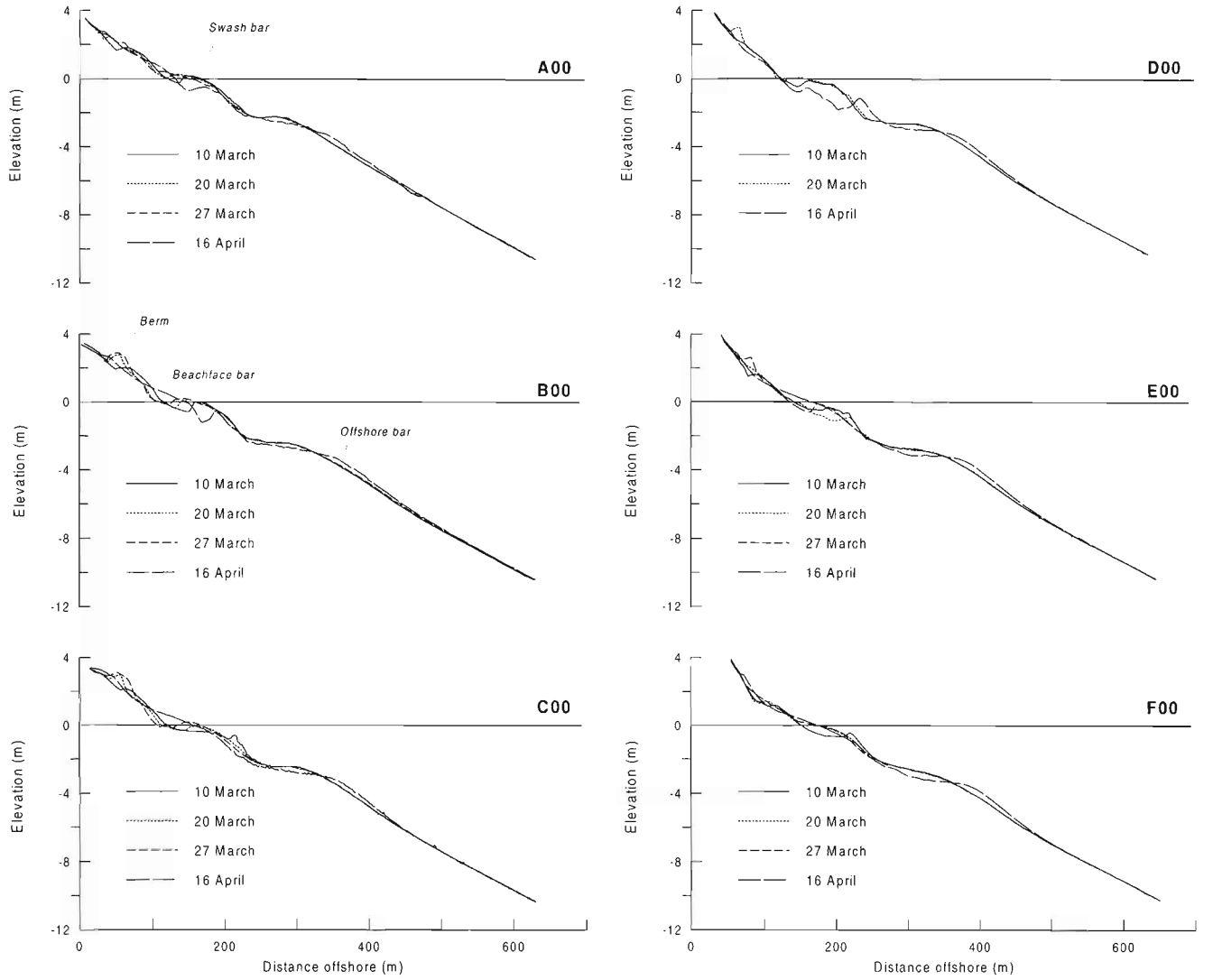

Figure 7. Beach-shoreface profiles surveyed by the sea-sled along the six primary profile lines, A00-F00.

lows, to set the context for the interpretations made of cross-shore fluxes and sand volume changes in the study swath.

Through March until the cyclone, the swath was characterised by four, largely shore-parallel bar features: an offshore bar, a swash bar, a beachface sandwave, and the beach berm. Superimposed on this were assorted bumps and holes associated with rip channels and upper-beach drainage, sometimes rhythmic topography on the beachface and swash bar, and a broad, shallow cuspate feature spanning the shoreface. Over this interval, the offshore bar (cresting the shoreface 2.5 m below MSL) remained generally static and is considered to be a remnant storm bar. The swash bar, lying on the lower beach at about MSL, began as a reasonably continuous and linear feature but was subsequently broken by two broad rip channels. These channels connected depressions in the adjacent troughs, and low deltas were deposited in the seaward trough (Figure 6). Through March, the swash bar migrated shoreward some 30–50 m and increased in elevation by about 0.3–0.6 m (Figure 7). A feature of the beachface over this period was that it exhibited considerable longshore variation in its topography and behaviour (Figures 6 and 7). The northern half of the beach lacked a significant area of berm early in March, but showed a beachface sandwave that pinched-out at about profile D00. From March 7, this sandwave migrated about 40 m up the beachface to form a steep, narrow berm by March 20. In contrast, the southern part of the beach began with an area of berm, a relatively steep beachface, and a flatter lower-beach, but berm buildup was delayed and weaker. The longshore change in behaviour coincides with the location of Mangawhai Forest behind profiles E00-F00, and may possibly relate to the effect of the forest on groundwater discharge to the beachface.

The broad cuspate feature on the shoreface, with a relief

of only 0.1–0.2 m and extending offshore to a depth of about 10 m, was only resolved by the de-trended topography (Figure 6). The 'horns' appearing along profiles A00 and F00 suggest a wavelength of about 500 m. This feature appeared to remain static through the study period.

The March 30–31 cyclone essentially flattened the beach, combing the berm and swash bars back into the troughs to seaward, and trimming the top of the offshore bar and spreading the eroded sand down the shoreface. The difference plot (Figure 6) shows a rhythmic change in deposition along the shoreface, with two apparent depositional lobes that line-up with post-storm holes/rip-channels on the lower beach. After the storm, divers observed aprons of cleaner sand draped down the shoreface over less well-sorted and more shelly sand—like frosting down the side of a cake. The sub-aerial beach showed a somewhat subdued, irregular topography by April 16, due to both the remnant form of the swash bar and storm-generated topography (such as holes, rip channels and their seaward deltas) that was evolving into crescentic and lingoid bars (Figure 6). Small, low-amplitude, discontinuous sand waves were also beginning to form on the beachface, prior to rebuilding the berm. On the northern half of the beach, berm sand was tossed higher as well as being combed seaward.

Thus, overall through the study period, the general pattern of beach change reflected mainly cross-shore sand transfers associated with the migration, formation, and destruction of the four shore-parallel bars. This was locally complicated by the effects of beach drainage channels and rhythmic topography, suggesting that the behaviour of a single profile may not necessarily represent that of the beach overall.

Shoreface Sand Level Changes and Scour Depths: Depth-of-Disturbance (DOD) Rod and Sled Comparison

Sand-level changes and maximum scour depths measured from the DOD rod arrays along the shoreface of profiles A00 and F00 (plus the sand-level changes from smoothed profiles surveyed with the sea-sled at the same locations) are listed in Table 2. For the first period, between early and mid March, along both profiles sand-level changes against individual DOD rods ranged over a few cm, with the average changes per station being approximately 1 cm. During both sets of measurements, the bed had symmetrical ripples with relief of up to 3–10 cm and wavelengths typically 20–30 cm. These bedforms account for the ranges observed and, along with measurement errors in reading the scale, could also induce an error of a few cm in the mean levels (given that there were only 5 sampling points at each station). In comparison, over the same time period and at the same locations, the smoothed sea-sled profiles indicated sand-level rises of up to 5 cm on profile A00 and falls up to 2 cm on profile F00, which differed from the mean DOD rod changes by 1–4 cm. Considering the ± 1 cm elevation uncertainty associated with the sled surveys and the measurement and sampling error associated with the DOD rod measurements, the two methods of fixing locally-averaged sea-bed levels are in agreement, and, to

Table 2. *Shoreface sand-level changes and scour depths measured by depth-of-disturbance (DOD) rods. The ranges indicate the minimum and maximum sand-level changes/scour depths among individual rods in each array. The sand-level changes measured by the sea-sled at the DOD rod locations are included for comparison. Bedforms around the rods at measurement times were either ripples (r) or hummocks (h). Horse-mussel patches (m) appeared in places after the March 30 storm. The figures in the bedform columns give maximum bedform heights (cm), e.g., r6/r3 indicates ripples up to 6 cm high during the first survey and up to 3 cm high on the second.*

Profile and Approx. Depth of DOD Rods (m below MSL)	Sand level changes (mm)							Scour depth (mm)	
	10 March–23 March				23 March–16 April			10 March–16 April	
	Bedforms	*Range*	*Mean*	*Sled*	*Bedforms*	*Range*	*Mean*	*Sled*	*Range*	*Mean*
A00-6	r6/r6	−24 to 0	−13	5	r6/h20	DOD rods lost		131	DOD rods lost	
A00-7	r5/r4	5 to 25	11	50	r4/r1 & m	−172 to 23	−90	−12	190 to 485	355
A00-8	r9/r5	−2 to 10	6	20	r5/h5	−95 to 25	−48	0	259 to 439	325
A00-9	r10/r4	−7 to 6	2	39	r3/r6	−34 to −12	−20	−21	172 to 274	227
A00-10	r10/r5	0 to 18	6	37	r10/r5	−17 to −1	−7	−3	88 to 294	204
F00-6	r6/r6	−1 to 11	2	−10	r7/r2	−157 to 156	44	171	163 to 483	349
F00-7	r8/r4	−9 to −1	−6	−17	r4/r6	−132 to 44	−17	2	175 to 381	278
F00-8	r6/r7	−25 to 28	9	−6	r7/r8	−23 to 31	4	15	213 to 288	263
F00-9	r6/r3	−1 to 5	−2	−17	r3/r4	−137 to 9	−58	6	282 to 442	345
F00-10	r6/r5	9 to 21	15	No data	r5/r7 & m	−109 to 0	−43	No data	247 to 267	257

within a cm or two, no significant changes in bed level are indicated at the DOD stations for this period.

For the second period, which included the 30–31 March storm, both the range of sand-level changes among individual rods and the mean sand-level changes of each array were larger, notably for the shallower stations (up to 20 cm range, 9 cm mean fall). However, the ranges were still within the limits possible from the bedforms and the mean changes were generally still within a few cm of those recorded by the sled. There were two exceptions to this. For one, on A00 at 7 m depth, only three DOD rods were left after the storm, so the standard error was large. For the other, on F00 at 6 m, the average was affected by a large fall against one rod. In both of these cases, similar changes in elevation were shown by the sled at the same depth on adjacent profiles, thus we conclude that the error induced in bed-level changes by measuring only a small number of rods in the presence of bedforms is greater than that associated with the sledding.

The maximum scour depths indicated by the washers placed on the DOD rods ranged up to almost 50 cm and averaged 20–35 cm, with a tendency for the average scour depth to decrease as water depth increased. These scour depths are consistent with the heights of the hummocky topography that was frequently recorded by the sled wheel during swell conditions on the seaward face of the outer bar (Figure 4b). Using the criterion of GREEN and BLACK (1999) for the transition from ripples to hummocky topography (*i.e.,* when the dimensionless skin friction due to waves, Θ', exceeds 0.14), hummocks would have been developed out to a depth of 37 m at the peak of the 30–31 March storm. Thus a probable explanation of the "scour and fill" history indicated by the washers is that it is the signature of a random field of mobile/transitory hummocks that developed during storm conditions then subsequently was smoothed out. There is no evidence that might support the alternative explanation of widespread scour and subsequent deposition over large spatial scales; on the other hand, since sledding was not possible during the cyclone, this cannot be discounted.

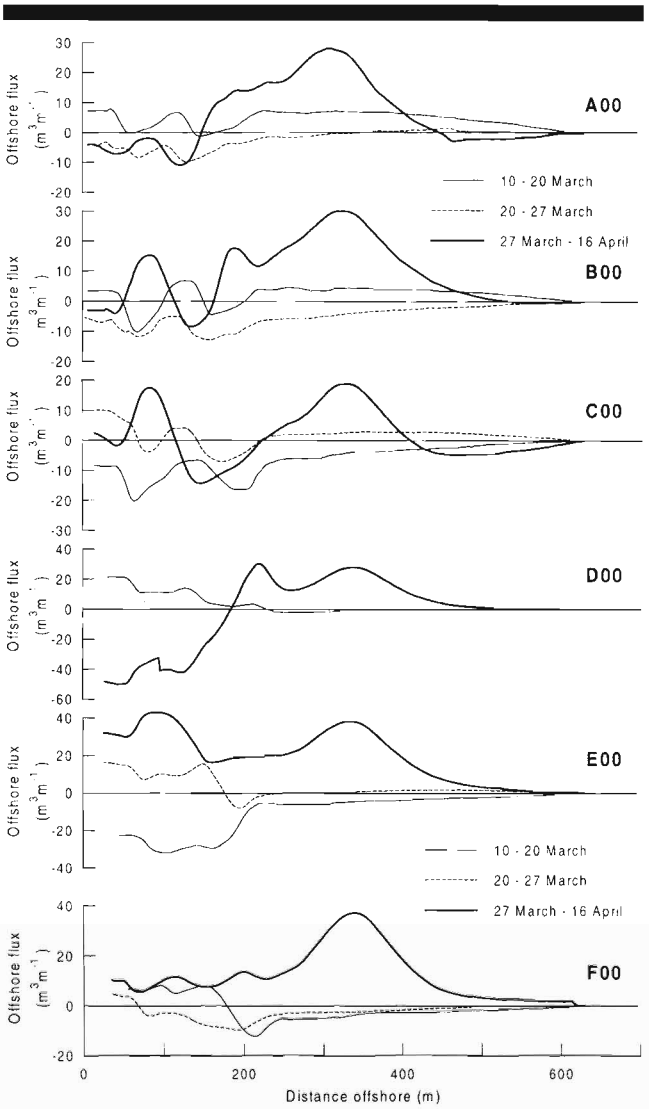

Figure 8. Distribution of cross-shore sand flux across primary profiles, A00-F00, as determined from integration of elevation changes between sea-sled surveys.

Cross-Shore Sand Fluxes Inferred from Profile Change

Distributions of net cross-shore sand flux across profiles A00-F00 (*i.e.* every third profile) for the periods between surveys, as determined from the surveyed elevation changes and equation (2), are plotted in Figure 8. Before interpreting these, however, it is instructive to consider what distributions might be expected for the "ideal" conditions of (i) a 2-d beach (with no longshore variation in sand fluxes), (ii) cross-shore transport pinching-out to zero going down the shoreface and landward of the beach berm, and (iii) perfectly accurate surveying.

On the basis of the general morphological changes discussed previously, for the March accretionary period the expected distribution might show (Figure 9b): weak, landward-increasing onshore transport on the shoreface; two onshore transport peaks associated with the shoreward migration of the swash bar and beachface bar; and zero flux or "volume closure" at the top of the beach, signifying no losses or gains of sand for the profile overall. For the period 27 March to 16 April, spanning the cyclone, the expected distribution might show (Figure 9b): offshore transport peaks associated with the flattening of the berm and swash bar and the seaward shift and build-up of the offshore (storm) bar; a seaward decrease in the offshore flux down the shoreface; and, again, zero flux at the top of the beach would indicate no losses of sand for the profile overall.

In practice, this ideal pattern will be complicated by accumulating errors in the integrated elevation changes and by longshore transport effects. While the uncertainty in fixing seabed elevation with the sea-sled is within ± 1 cm, if this error is systematic then the accumulated error or "drift" in the flux may be up to 2 m^3m^{-1} per 100 m length of profile (i.e. up to 12 m^3m^{-1} for the total 600 m length). Also, since the fundamental assumption with the method is that the elevation changes across the profile are due only to cross-shore

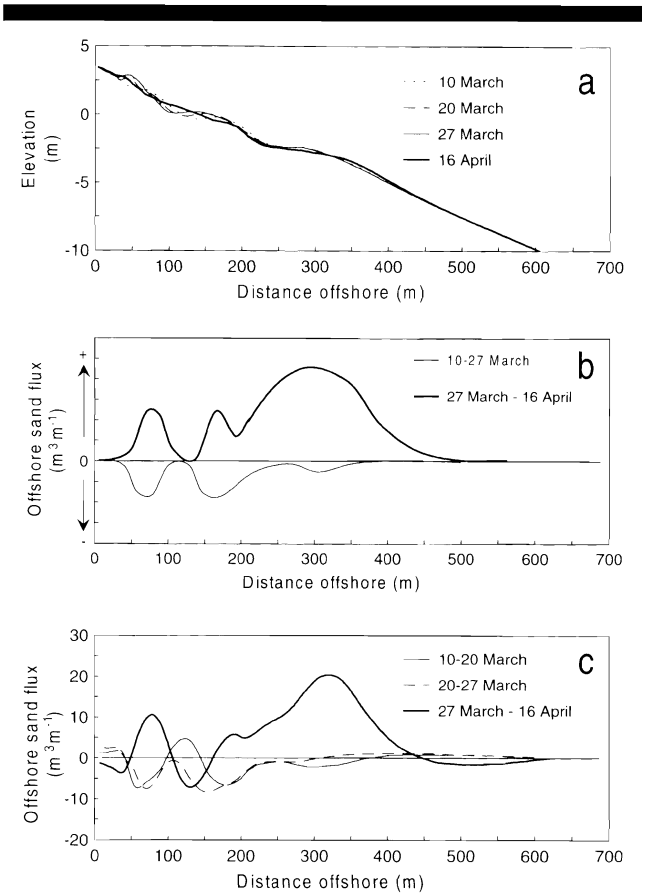

Figure 9. (**a**) Beach-shoreface profiles obtained by averaging the seven profiles between A00 and C00. (**b**) Distribution of cross-shore sand flux (not to scale) expected for ideal conditions of a 2-d shore with no sand losses or gains. (**c**) Actual distribution of cross-shore sand flux over the averaged profile.

gradients in the cross-shore transport rate, then any elevation change due to a gradient in longshore transport (such as relating to rip current cells and rhythmic topography) will locally corrupt the integration. These accumulating measurement errors and 2-d transport effects may confuse the local net cross-shore transport and any net flux across the boundaries (*i.e.* offshore to the inner shelf or onshore into the sand dunes).

The actual flux distributions (Figure 8) show features of the expected patterns but are more complicated and typically show a "drift" which results in a greater or lesser volume misclose. Profile B00 reasonably follows the expected trend, particularly if the drift is removed by "eye". For both the accretion and erosion periods, the misclose in the volume change integrated over the profile was only 2–3 m^3m^{-1}, suggesting an essentially 1-dimensional exchange of sand that was contained between the beach and upper shoreface, with negligible exchange further offshore. A small systematic error in the March 20 survey (approximately 1 cm elevation) appears to be recovered by the March 27 survey, but this could also relate to slight changes in the mega-cuspate shoreface feature.

Profile D00 shows the most unexpected flux pattern. The apparent instances of offshore transport in mid March and onshore (*i.e.,* negative offshore) transport into April on the beach segment of the profile (*i.e.,* landward of 200 m, Figure 8) almost certainly relate to 2-d transport associated with the rip channel that developed there (*c.f.* Figure 6). The substantial volume miscloses (30 m^3m^{-1} for 20 March–16 April) at profile E00 probably relate to the same effect. At F00, however, the volume miscloses are smaller and the sand transfers again appear to relate mainly to cross-shore transport.

To minimise the effects of survey errors, 3-d features, and longshore-transport gradients, the seven northernmost profiles (where the beach behaviour was more uniform) were merged into a single profile by averaging their elevations along the shoreline trend (Figure 9a). The cross-shore fluxes derived from this (Figure 9c) confirm the expected multi-peak patterns described above. Notably, the volume miscloses at the top of the beach are small, no more than 2.8 m^3m^{-1}per inter-survey interval, and they appear to stem largely from the flux inferred across the lower shoreface. This area, because of its range from the shore-based EDM, is most sensitive to surveying errors and it is likely that these "fluxes" are artifacts (the miscloses would disappear substantially if the integration was begun at an offshore distance of 500 m). Of further note are: (i) during March, as well as the two main onshore transport peaks (about 15 m^3m^{-1} in total) at the swash bar and upper beachface, there was an additional but relatively small onshore transport peak (about 2 m^3m^{-1}) at the outer bar; (ii) the peak offshore transport during the cyclone period (about 30 m^3m^{-1}) was associated with the outer bar, with the transport then decreasing exponentially seawards to become negligible at about 8 m water depth; (iii) local flux minima suggest that the two transport belts over the swash bar and on the upper beachface were substantially decoupled from each other during both accretion and erosion phases (*i.e.,* the net transfers of sand between the sub-aerial beach and offshore were small compared to the local transfers), while offshore "leakage" of sand between the swash bar and outer bar is indicated during the erosion phase.

Sand Volume Changes

The volume miscloses in the cross-shore fluxes, equal to the net gain in volume under the profiles, are summarised in Table 3. They range from 0 to 48 m^3m^{-1} between successive surveys. The largest occur at profiles D00 and E00, not unexpectedly owing to the occurrence of rip channels in this segment. When the volume changes over the six primary profiles (i.e., A00, B00, . . . F00) are averaged, the volume change reduces to 1.3, 3.6, and -1.9 m^3m^{-1} for the three successive survey intervals. These figures equate to total volume changes within the 500 m × 630 m swath of 670, 1810, and -930 m^3, or to mean elevation changes of 2.1, 5.7, and -2.9 mm, respectively. For the March 10–20 interval, when 14 profiles were resurveyed, the average volume change reduced to 0.59 m^3m^{-1} (0.9 mm). The seven northern profiles (*i.e.,* A00, A30, ... C00) show average volume changes over the three inter-

Table 3. *Net sand volume changes under profiles (integrated across shoreface and beach) between consecutive surveys. First set of results is for the six primary profiles (A00, B00, . . . F00, as located on Figure 2), spanning the whole study shore. Second set is for al seven profiles on the norther part of the beach (i.e., A00, A30, . . . C00, Figure 2).*

Distance North (m)	Profile	Volume change (m^3 per m length of shore)		
		March 10–20	March 20–27	27 March–16 April
500	A00	7.46	−3.96	−4.7
400	B00	3.52	−5.43	−3.06
300	C00	−8.26	10.2	2.5
200	D00	21.4	0	−48.2
100	E00	−22.8	16.3	31.9
0	F00	6.74	4.68	10.4
	Average	1.35	3.62	−1.86
500	A00	7.46	−3.96	−4.7
470	A30	−1.17	−5.03	14.1
430	A70	−5.61	10.6	18.0
400	B00	3.52	−5.43	−3.06
370	B30	9.84	8.47	−6.9
330	B70	0.97	1.78	−9.49
300	C00	−8.26	10.2	2.5
	Average	0.97	2.38	1.49

vals of 1.0, 2.4, and 1.5 m^3m^{-1} (1.5–3.8 mm). Such volume changes, involving mean elevation changes of only a few mm, are negligible and within the bounds of measurement error (note that with the mean cross-shore slope of 0.02, a 2 mm elevation change involves a shore translation of only 0.1 m).

Thus, cross-shore sand fluxes and volume miscloses found by integrating elevation changes along a single profile may be quite misleading and unrepresentative due to longshore transport gradients associated with even subdued 3-d topography and to surveying errors as small as ± 1 cm in elevation. However, when multiple profiles spanning the 3-d topography are averaged, the underlying pattern of cross-shore transport emerges and the volume misclose decreases substantially.

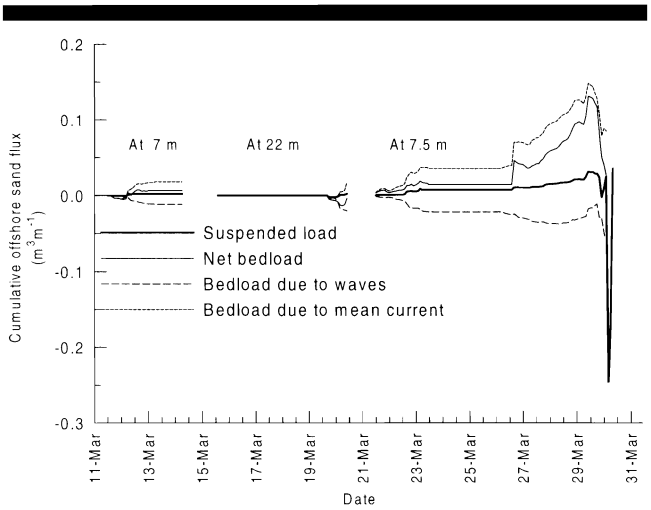

Figure 10. Cumulative cross-shore sand flux determined from *Alice* instruments at 7 m, 22 m, and 7.5 m depth stations near line of profile A00. Bedload due to the mean current is the difference between net bedload, computed using the total current, and bedload due only to the orbital motion of waves, obtained by subtracting mean current from total current.

Alice Results

Net cross-shore sand fluxes due to suspended and bedload transport, as estimated from the *Alice* data using equations (3) and (7) and accumulated for the three *Alice* deployments over 11–31 March, are plotted in Figure 10. The bedload components due to orbital asymmetry and to the mean current are plotted as well as the total bedload.

Except during the March 30–31 storm, bedload prevailed over suspended load and weak offshore mean currents largely balanced episodes of onshore forcing by wave orbital-velocity asymmetry, resulting in very small net fluxes. For example, over the deployment at 7 m depth from 11–14 March, the net bedload flux was less than 0.01 m^3m^{-1} and the suspended flux was essentially zero. At 22 m depth, no transport at all was indicated until the small wind-wave event on 19–20 March. At 7.5 m depth, several small transport episodes up until 29 March induced a net offshore bedload flux of 0.1 m^3m^{-1} with a net offshore suspended flux approximately one tenth as large. These tiny flux values are less than those measured by the sea-sled, but are also well within the margin of error afforded by the sea-sled method.

During the storm of 30–31 March, by late morning on 30 March the significant wave height was over 2.8 m and the dimensionless skin friction (Θ') exceeded 0.6, thus it was no longer possible to reliably estimate C_o in equation (4) from GREEN and BLACK's (1999) model (which was established only for $\Theta' \leq 0.6$). By that stage too, the ABS signal had become saturated and so it became impossible to estimate the suspended load. However, until that stage, the *Alice* data indicated a phase of onshore bedload, due both to wave asymmetry and onshore net currents, and an increasingly predominant suspended load whose cumulative net cross-shore flux switched between onshore and offshore as the current direction changed. Some uncertainty must be attached to the plot-

ted net fluxes because of the uncertainty in current meter orientation (which was fixed to ± 5 degrees at best and affects the resolution of the cross-shore component). At times, there were strong longshore components to the mean currents, and these may have "leaked" into the cross-shore components. Nonetheless, the indication from the *Alice* instruments, while they remained functional during the early stages of the storm, was that the net cross-shore fluxes were relatively small, which is in accord with the net offshore flux of < 1 m^3m^{-1} at 7.5 m depth on the "average profile" as determined from the March 27 and April 16 sea-sled surveys.

In summary, the *Alice* data showed very small net sand fluxes across the shoreface at 7 m depth or greater through the various wave conditions experienced in March, which is consistent with the flux estimates based on the sea-sled surveys. This supports the concept of using the *Alice* instruments to measure sand fluxes further offshore, beyond the 13 m depth-limit of the sea-sled.

DISCUSSION

Sand Exchanges Between the Shoreface and Inner Shelf at Mangawhai

HESP and HILTON (1996) concluded, from mainly morphological and sedimentological evidence, that in the long-term the beach-sand wedge in the Mangawhai-Pakiri embayment is essentially a closed system, with insignificant sand gains from or losses to offshore. Our localised and short term experimental study, although obviously not claiming to be representative of the "long-term", lends some support to this conclusion. This support includes the direct measurements by *Alice* showing negligible net cross-shore flux on the outer shoreface during swell conditions, and the exponential decay down the shoreface of profile change and inferred cross-shore fluxes obtained from the sea-sled measurements after periods of swell-driven accretion and storm erosion. While the net overall volume changes in the study swath between surveys range from -1.9 to $+ 3.6$ m^3m^{-1} (Table 3), these cannot be interpreted unequivocably as sand gains or losses since they incorporate surveying and sampling errors of the same order (although net sand exchanges within this margin also cannot be excluded). We would only expect to be able record statistically significant volume changes to/from our study swath by monitoring over a longer period of time. For example, our approximately 4 m^3m^{-1} uncertainty in beach-shoreface volume detection equates to a detection threshold of 40,000 m^3 for the 10 km span of Mangawahi Beach. If the annual natural sand renourishment to this span of beach from offshore is the order of 6,000 m^3y^{-1}, as indicated from the numerical modelling by HUME *et al.* (1999), then in order to detect this we would need to monitor our swath for at least seven years, preferably several times that interval, with no less detail than employed in this study.

Effect of Bedforms on Accuracy of Sea-Sled Surveying

An unexpected but important finding from the sea-sled surveys was how the elevation at the base of the sled could be biased from the true local mean seabed elevation due to the track taken by the sled runners through bedforms. As shown by the digitising wheel on the sea-sled, this bias varied spatially, in both sign and magnitude, depending on the firmness of the sand and the type of bedform. With ripples the bias was only a few mm. However, with hummocky bedforms it was as large as several cm and, if uncorrected, when integrated across profiles it would have induced errors of up to 13 m^3m^{-1} in the sand volume and would have corrupted the magnitude and possibly the direction of cross-shore flux estimates. Thus for precision surveys of sand-level change with a sea-sled, an on-board sensor that records the position of the sled base relative to the sea-bed (whether a wheel such as we used or a high-resolution sounder) would appear to be mandatory.

Longshore Variation in Beach Morphology and Processes—Implications for Sand Flux and Volume Estimates and for Profile Surveys Generally

Another lesson from the study is that cross-shore sand fluxes and volume changes found by integrating elevation changes along a single profile could be quite misleading and unrepresentative, due to longshore transport gradients associated with even subdued 3-d topography. However, when multiple profiles spanning the 3-d topography were averaged, the underlying pattern of cross-shore transport emerged and the volume misclose across the profile decreased substantially.

This has general implications for using profiles to monitor beaches that show morphodynamic states similar to those observed at Mangawhai, either for the purpose of monitoring sand volumes or for calibrating or verifying models that predict the spatial distribution of cross-shore transport from wave data. In either application, a single profile or a few profiles spaced further apart than the characteristic spacing of the 3-d beach morphology (*e.g.,* every 2 km along a 10 km beach) may poorly represent the beach as a whole. A comprehensive survey of the entire beach-shoreface at sufficient spatial detail is ideally required, but is usually prohibitively expensive. An acceptable compromise is to focus on representative swaths that are wide enough to capture the typical 3-d morphology. Unlike more widely spaced profiles, variations among profiles within the swath(s) should substantially average-out. It follows that a good appreciation should be gained of the scaling characteristics of beach-shoreface morphologies before such swaths are designed. Since most of the 3-d relief tends to appear on the intertidal beach, photogrammetry offers an excellent tool for such reconnaissance mapping.

Comparison with Hallermeier's Depth Limits for Profile Activity

It is useful to compare the patterns of profile change and sand fluxes on the shoreface at Mangawhai with the depth limits of HALLERMEIER's (1981) "shoal" zone, *i.e.,* the area of shoreface over which "significant" but not intensive on-offshore transport occurs. According to Hallermeier, the *seaward* limit of the shoal zone signifies the maximum depth at which low swell mobilises sand and starts to scrape it shoreward. Hallermeier recommended using the local median

wave condition (from at least one year of wave record) to represent this conceptual swell condition. He suggested that this seaward depth limit, d_i (with respect to mean low water datum), could be approximated by

$$d_i \cong (H_s - 0.3\,\sigma)T_s\,(g/5000D)^{0.5} \quad (10)$$

where D is the shoreface sand size (0.2 mm at Mangawhai) and σ is the standard deviation of H_s. $H_s - 0.3\,\sigma$ is Hallermeier's approximation for the median wave height.

Hallermeier deemed the *landward* limit of his shoal zone as the maximum depth for erosive cutting of the nearshore by the yearly extreme waves, and considered that this should be consistent with the yearly profile closure depth (*i.e.,* where repeat surveys merge to within the margin of survey error—which, at the time, was of the order of 0.3 m based on echosounding). He suggested that this depth limit, d_l, could be approximated by

$$d_l \cong 2(H_s + 5.5\,\sigma) \quad (11)$$

where $H_s + 5.5\,\sigma$ approximates the 0.137^{th} percentile significant wave height for the record period (corresponding to the H_s that is exceeded for 12 hours during one year).

Table 1 shows these wave statistics at the Mangawhai buoy and the resultant values of d_i and d_l (corrected to the MSL datum) for two periods: the 9 March–16 April 1996 period of intense beach profile surveying and the whole 32 month record from the wave buoy (the wave height statistics have been transformed from the 35 m depth at the wave buoy to the d_i and d_l depths by iteration using linear shoaling theory). The wave statistics for both periods are very similar, suggesting that the study period is representative of the longer record. The d_i estimated for the 1996 study period was 10.7 m. This is reasonably consistent with the field measurements. The *Alice* deployments showed no significant cross-shore transport under swell conditions at 12 m and 20 m depth but did show weak transport at 7 and 7.5 m depth. The sea-sled measured profile changes through March suggested no (measurable) net cross-shore fluxes at depths greater about 5 m (Figure 9c).

The d_l estimated for the 1996 study period was 8 m, based on the peak wave conditions on 30 March. This certainly corresponds to the surveyed closure depth of 7–8 m (Figures 6 and 7). While the DOD rod records showed that at 7 m depth the bed was being worked over to a sand depth of 0.3–0.4 m, this was in association with the formation of hummocky bedforms, and the net sand level changes over the storm, after these bedforms had been flattened out again, were within the few cm measuring limits of the sea-sled. Thus Hallermeier's model correctly predicted the depth of beach profile closure at Mangawhai due to the extreme waves.

Finally, the depth limits for Hallermeier's shoal zone given in Table 1 should not necessarily be regarded as representative of the Mangawhai coast in the long term. This is because the period of wave record generally spanned the more storm-prone La Nina phase of the Southern Oscillation. During El Nino phases of the Southern Oscillation, the shoal zone might be expected to extend further shoreward.

SUMMARY AND CONCLUSIONS

The main findings of this study are:

(1) During the six weeks of monitoring, the study swath of beach underwent swell-driven accretion, erosion by storm waves, and partial recovery. During the swell phase, the beach began with a longshore-bar-and-trough form, and bars in the swash zone and on the upper beachface migrated shoreward. As this phase proceeded, a mildly rhythmic beach topography developed as rip channels cut through the swash bar. The storm waves flattened the beach and shifted the outer bar seaward, casting aprons of sand down the shoreface.

(2) With our sea-sled system, we were able to survey sand-level changes on the shoreface to about ± 1–2 cm accuracy, as demonstrated by repeat surveys on consecutive days and by comparison with sand level changes against rods in the seabed. The digitising wheel on the sea-sled often showed a bias of the elevation of the base of the sled from the true local mean seabed elevation due to the track taken by the sled runners through bedforms. This bias varied in sign and magnitude depending on the firmness of the sand and the type of bedform, and was as large as several cm over hummocky bedforms. If uncorrected, this would have induced substantial errors in the sand volume under profiles and in inferred cross-shore sand fluxes.

(3) Cross-shore sand fluxes determined from the surveyed changes in sand levels showed an overall pattern of onshore transport during swell episodes and offshore transport during the storm. The swell-driven onshore transport was substantially confined to the beach, involving the shoreward-migration of a swash bar and a sandwave on the upper beachface. The offshore transport during the storm was greatest under the outer bar and decayed exponentially seaward, pinching-out at a depth of about 7–8 m on the shoreface. This average pattern was confused at some profiles, mainly due to non-uniform longshore transport associated with 3-d features such as rip channels and rhythmic topography, but probably also to a lesser degree by accumulating survey errors.

(4) While sand volume changes under individual profiles were sometimes large between surveys, the overall changes in sand volume in the study swath were small (ranging from 1–4 m^3m^{-1}) and consistent with the surveying and sampling errors. This small misclose, together with the closure of sand-level changes on the shoreface and the small sand fluxes measured by the instrument tripod during swell on the shoreface, suggest that little sand exchange occurs between the shoreface and inner shelf. While these observations are limited in space and time, they are nonetheless consistent with previous conclusions made from sedimentological evidence and hydrodynamic modelling that the beach-shoreface in the Mangawhai area receives relatively little sand renourishment from the inner shelf.

(5) The measured profile closure depth at Mangawhai is consistent with the landward depth limit of Hallermeier's (1981) shoal zone.

ACKNOWLEDGEMENTS

Thanks to Rod Budd, Andy Hill, Aleki Taumoepeau, Sabina Rodda, Bob Tasker, and Graeme Mckay, from the National Institute of Water and Atmospheric Research in Hamilton and Whangarei, for assistance in the field. Thanks also to Gail and Box for memorable accommodation. Terry Hume provided constructive comment on the manuscript. The study was funded by the Foundation for Research, Science and Technology under contract CO1511.

LITERATURE CITED

BAILARD, J.A., 1981. An energetics total load sediment transport model for a plane sloping beach. *Journal of Geophysical Research,* 86 (C11), 10938–10954.

BLACK, K.P.; BELL, R.G.; OLDMAN, J..O.; CARTER, G.S., and HUME, T.M., 2000. Features of 3-dimensional barotropic and baroclinic circulation in the Hauraki Gulf, New Zealand. *New Zealand Journal of Marine and Freshwater Research,* 34, 1–28.

BLACK, K.P.; OSBORNE, P.D.; GREEN, M.O., and VILLARD, P.V., 1997. Intra-wave suspended sediment concentrations over bedforms. *In: Pacific Coasts and Ports '97,* Proceedings, Combined Australasian Coastal Engineering and Ports Conference, Christchurch, pp. 365–370.

EMERY, K. O., 1961. A simple method for measuring beach profiles. *Limnology and Oceanography,* 6, 90–93.

ENRIGHT, N. J. and ANDERSON, M. J., 1988. Recent evolution of the Mangawhai Spit dunefield. *Journal of the Royal Society of New Zealand,* 18 (4), 359–367.

GIBB, J.G., 1978. Rates of coastal erosion and accretion in New Zealand. *New Zealand Journal of Marine and Freshwater Research,* 12, 429–456.

GREEN, M.O., 1996. Introducing Alice. *Water & Atmosphere,* 4 (2), 8–10.

GREEN, M.O., 1999. Test of initial-motion theories using irregular-wave field data. *Sedimentology,* 46, 427–441.

GREEN, M.O. and BLACK, K.P., 1999. Suspended-sediment reference concentration under waves: field observations and critical analysis of two predictive models. *Coastal Engineering,*38, 115–141.

GUZA, R.T. and THORNTON, E.B., 1985. Velocity moments in nearshore. *A.S.C.E., Journal of Waterways, Port, Coastal and Ocean Engineering,* 111, 235–256.

HALLERMEIER, R.J., 1981. A profile zonation for seasonal sand beaches from wave climate. *Coastal Engineering,* 4, 253–277.

HESP, P. and HILTON, M.J., 1996. Nearshore-surfzone system limits and the impacts of sand extraction. *Journal of Coastal Research,* 12 (3), 726–747.

HICKS, D.M. and GREEN, M.O., 1997. The 'fall-speed parameter' as an index of cross-shore sand transport: verification from measurements on the shoreface. *In: Pacific Coasts and Ports '97,* Proceedings, Combined Australasian Coastal Engineering and Ports Conference, Christchurch, pp. 1089–1094–370.

HILTON, M.J., 1995. Sediment facies of an embayed coastal sand body, Pakiri, New Zealand. *Journal of Coastal Research,* 11 (2), 529–547.

HUME, T.M.; BELL, R.G.; BLACK, K.P.; HEALY, T.R., and NICHOL, S.L., 1999. Sand movement and storage and nearshore sand extraction in the Mangawhai-Pakiri embayment. Mangawhai-Pakiri Sand Study Final Report, NIWA Client Report ARC60201/10, National Institute of Water and Atmospheric Research Limited, Hamilton, October 1999, 80 p.

HUME, T.M.; OLDMAN, J.W., and BLACK, K.P., 2000. Sediment facies and pathways of sand transport about a large deep water headland, Cape Rodney, New Zealand. *New Zealand Journal of Marine and Freshwater Research,* 34, 695–717.

INMAN, D.L. and BAGNOLD, R.A., 1963. Littoral processes. *In: The Sea: Ideas and Observations,* vol. 3, Interscience Publishers, New York, New York, pp. 529–533.

KOMAR, P.D. and MILLER, M.C., 1973. The threshold of sediment movement under oscillatory water waves. *Journal of Sedimentary Petrology,* 43, 1101–1110.

LARSEN, M. and KRAUS, N.C., 1989. *SBEACH: numerical model for simulating storm-induced beach change, Report 1, empirical foundation and model development,* Technical Report CERC-89-9, US Army Corps of Engineers, Vicksburg, Mississippi, 256 p.

MCCABE, P., 1985. Mangawhai harbour and the development of its dual inlet system. M.Sc. thesis, University of Waikato, Hamilton, 216 p.

NORTHLAND REGIONAL COUNCIL, 1988. Coastal hazard identification Whangarei County. Northland Regional Council, Whangarei, Technical Publication No. 1988/1, 97p.

NORTHLAND REGIONAL COUNCIL, 1991. Coastal hazard identification in former Mangonui County area. Northland Regional Council, Whangarei, Technical Publication No. 1991/3, 58p.

SCHOFIELD, J.C., 1970. Coastal sands of Northland and Auckland. *New Zealand Journal of Geology and Geophysics,* 13, 767–824.

SMITH, R.K.; LATIMER, G.J.; SWALES, A.; RUTHERFORD, J.C.; BUDD, R.G.; OVENDEN, R., and HAMBLING, J., 1997. Nearshore profile and bedform measurements using an enhanced sea sled survey technique. *Shore & Beach,* 65(4), 15–22.

SOULSBY, R.L., 1983. The bottom boundary layer of shelf seas. *In:* JOHNS, B. (ed), *Physical Oceanography of Coastal and Shelf Seas,* Elsevier, Amsterdam, pp. 189–266.

STERNBERG, R.W., 1972. Predicting initial motion and bedload transport of sediment particles in the shallow marine environment. *In:* SWIFT, D.J.P.; DUANE, D.B., and PILKEY, O.H. (eds), *Shelf Sediment transport: Process and Pattern.* Dowden, Hutchinson and Ross, Stroudsburg, Pennsylvania, pp. 6–82.

SWALES, A., submitted. Geostatistical estimation of short-term changes in a beach sand budget, Mangawhai, New Zealand. *Journal of Coastal Research.*

WRIGHT, L.D. and SHORT, A.D., 1984. Morphodynamic variability of surf zones and beaches: a synthesis. *Marine Geology,* 56, 93–118.